Origin of the Enhanced Photoluminescence Quantum Yield in $MAPbBr_3$ Perovskite with Reduced Crystal Size

Nikolaos Droseros,[†,‡] Giulia Longo,[#] Jan C. Brauer,[‡] Michele Sessolo,[#] Henk J. Bolink,[#] and Natalie Banerji*[,†,‡,§]

[†]Department of Chemistry and Biochemistry, University of Bern, Freiestrasse 3, CH-3012 Bern, Switzerland
[‡]Department of Chemistry, University of Fribourg, Chemin du Musée 9, CH-1700 Fribourg, Switzerland
[#]Instituto de Ciencia Molecular, Universidad de Valencia, Catedràtico José Beltràn 2, 46980 Paterna, Spain

Supporting Information

ABSTRACT: Methylammonium lead bromide perovskite ($MAPbBr_3$) has been widely investigated for applications in visible perovskite light-emitting diodes (LEDs). Fine-tuning of the morphology and of the crystal size, from the microscale down to the quantum confinement regime, has been used to increase the photoluminescence quantum yield (PLQY). However, the physical processes underlying the PL emission of this perovskite remain unclear. Here, we elucidate the origin of the PL emission of polycrystalline $MAPbBr_3$ thin films by different spectroscopic techniques. We estimate the exciton binding energy, the reduced exciton effective mass, and the trap density. Moreover, we confirm the coexistence of free carriers and excitons, quantifying their relative population and mutual interaction over a broad range of excitation densities. Finally, the enhanced PLQY upon crystal size reduction to the micro- and nanometer scale in the presence of additives is attributed to favored excitonic recombination together with reduced surface trapping thanks to efficient passivation by the additives.

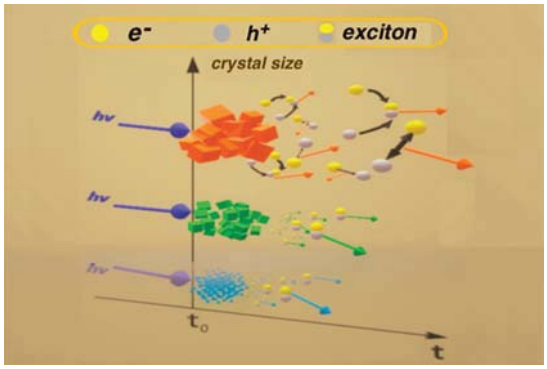

Hybrid organic–inorganic perovskites are emerging as highly promising new-generation energy materials. They are intensively studied for photovoltaic applications, thanks to their high absorption coefficients, low exciton binding energies, and high carrier mobilities.[1−3] In addition, aiming to reduce the global energetic consumption, perovskites with higher exciton binding energies, wider band gaps, and narrow emission bandwidths are excellent candidates for energy-efficient photonic and optoelectronic applications, such as light-emitting diodes (LEDs).[4−8] Methylammonium lead bromide ($MAPbBr_3$) is the most studied perovskite for LEDs due to its easy thin-film processing and its green emission. However, the low photoluminescence quantum yield (PLQY) of $MAPbBr_3$ limits its use in efficient light-emitting applications. The main strategy to foster the emission in this material has been the control over the crystal growth, in particular, by limiting the grain size to the micro- and nanoscale.[9−11] Despite growing knowledge about the perovskite morphology and its optoelectronic performance, the physical mechanisms governing the PL in $MAPbBr_3$ thin films remain unclear. Both free carriers[12] and excitons[13] have been suggested as the emissive species, but their interplay has been studied only at high carrier densities[14] and recently at low temperature.[15] Moreover, a systematic correlation between the reduction of the crystal size and the origin of the enhanced PLQY is missing. In this context, the dependence of the PL properties on the excitation density needs to be examined more exhaustively because it brings insights about the origin of the PL.[16,17]

Here, we elucidate the PL properties of solution-processed perovskite thin films with different morphologies and crystal grain sizes by steady-state and time-resolved spectroscopy. Three different systems are compared: neat polycrystalline $MAPbBr_3$ (grain size on the order of ∼1 μm), a polymer–$MAPbBr_3$ blend with crystal size in the tens to hundreds of nanometer range (50 ± 25 nm; see the SEM image in Figure S1),[18] and a small molecule–$MAPbBr_3$ blend with crystal size in the weak quantum confinement regime (9.1 ± 1.6 nm; see the TEM image in Figure S1).[9] All of the material preparation (compound storage, solution preparation, thin film deposition)

as well as the photophysical characterization is described in the SI and was carried out in an inert atmosphere. For simplicity, the samples will be referred to as "polycrystalline perovskite", "microcrystals", and "nanocrystals". We show the coexistence of both free carriers and excitons in the polycrystalline perovskite and monitor their interaction over a broad range of excitation densities. We also find that the increased PLQY with crystal size reduction is due to a bright exitonic population even at low excitation density, together with reduced surface trapping thanks to passivation by the additives.

Figure 1a shows the steady-state PL and absorption spectra of the three $MAPbBr_3$ thin films. Both the absorption onset and

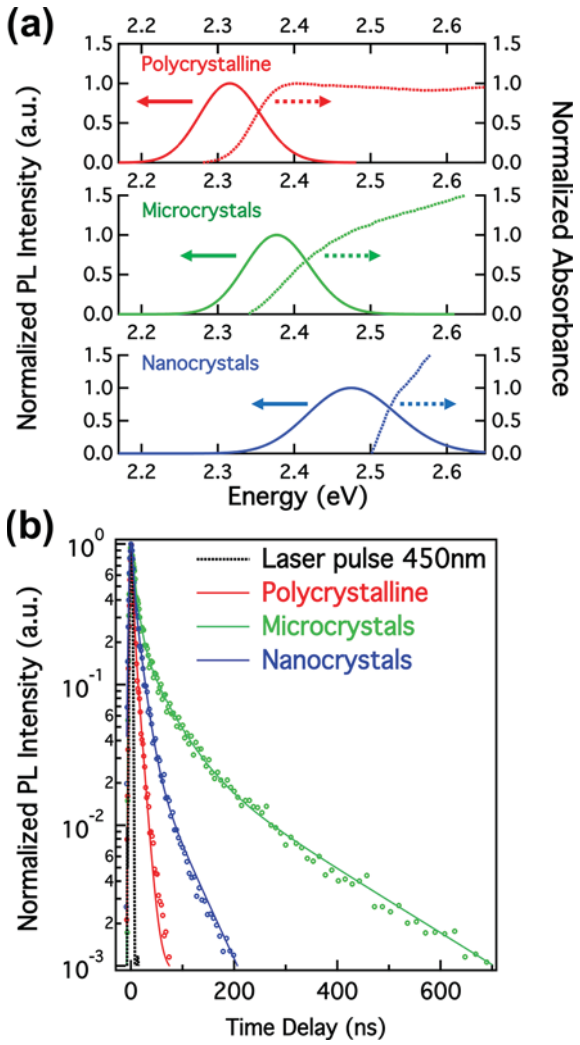

Figure 1. (a) Steady-state PL (left) and absorption spectra (right) and (b) TRPL dynamics of the three samples, recorded with excitation at 450 nm with 3 ns duration pulses and a repetition rate of 10 Hz at a common carrier density of ~10^{16} cm^{-3}. The detection is at the wavelength of the maximum PL intensity.

PL bands are blue-shifted as the size of the perovskite crystals decreases. The exciton Bohr radius of the bulk material has been reported to be 2 nm,[19] while Malgras et al.[20] observed a quantum confinement effect in $MAPbBr_3$ crystals with a diameter up to 7.1. nm. The average size of our nanocrystals, 9.1 ± 1.6 nm, can thus justify the existence of weak quantum confinement and the subsequent blue shift compared to the bigger crystals and grains. On the other hand, the blue shift observed for the microcrystals cannot be attributed to quantum confinement.[21] Two other possible explanations can be given. First, a change in the dielectric screening of the excitons induced by the presence of the additive (see Table S1 in the SI) could lead to the blue shift.[22] Second, according to Grancini et al.,[23] a stronger distortion in the Pb–I bond has been observed upon crystal size reduction in $MAPbI_3$, and D'Innocenzo et al. attributed the PL blue shift in ~100 nm crystals to this strain effect.[24] The lack of a clear excitonic feature in the absorption spectra as well as the broad PL peaks points to a rather broad distribution of particle sizes in the micro- and nanocrystalline materials (as confirmed in Figure S1).

Figure 1b shows the time-resolved photoluminescence (TRPL) dynamics of the three samples under similar excitation density (as calculated in the SI). A difference in the PL dynamics obtained at different positions of the same sample has been reported in previous studies.[25,26] In our study, the probed area was too large (8 mm laser spot; see Table S2 in the SI) to distinguish any local variation of the excited-state deactivation dynamics, and the results are an average over the microscale inhomogeneity. The PL decay for the micro- and nanostructured films is slower compared to that for the polycrystalline material, which, together with a higher oscillator strength for the emission, can contribute to the much higher PLQY (increase from 1.2 to 80%; Table 1). This trend contradicts

Table 1. Average PL Lifetime, PLQY, and Radiative and Nonradiative Recombination Rate Constants for the Perovskite Film Series

sample	τ_{av} (ns)	PLQY (%)	$k_{rad} \times 10^7$ (s^{-1})	$k_{n.rad} \times 10^7$ (s^{-1})
polycrystalline perovskite	5.4	1.2	0.22	18.2
microcrystals	21.4	80	3.73	0.93
nanocrystals	12.3	80	6.5	1.62

previous reports of faster dynamics in nanocrytsals,[20,24] which we discuss below in terms of traps. The average PL lifetimes are reported in Table 1, together with the radiative (k_{rad}) and nonradiative recombination ($k_{n.rad}$) rate constants. The increase of the PLQY in the micro- and nanocrystals correlates with an increase in k_{rad} (higher oscillator strength) and a decrease in $k_{n.rad}$. Radiative processes include direct band-to-band recombination such as exciton recombination or free electron–hole recombination. Nonradiative recombination can occur if excitons or free carriers are trapped, via exciton–exciton annihilation or by three-body Auger processes involving free charges.

The time-integrated PL spectra of the three samples were collected at different excitation densities, under excitation with pulses of 3 ns duration at 450 nm. Interestingly, the integrated PL spectra of the micro- and nanocrystals were found to be independent of the excitation density, while a clear change in the spectral shape was observed for the polycrystalline film (Figures 2a and S2). A possible explanation for this behavior might be reabsorption due to an increased penetration depth,[27,28] but we exclude this here as the thickness of the perovskite film is only 60 nm. Furthermore, a change in the PL spectra due to photodegradation of the sample with increasing excitation density was excluded because we showed repeatability of the observations when measuring the data again on the same sample spot at zero time delay t_0 (see Figure S3). We also found that the emission properties do not change under

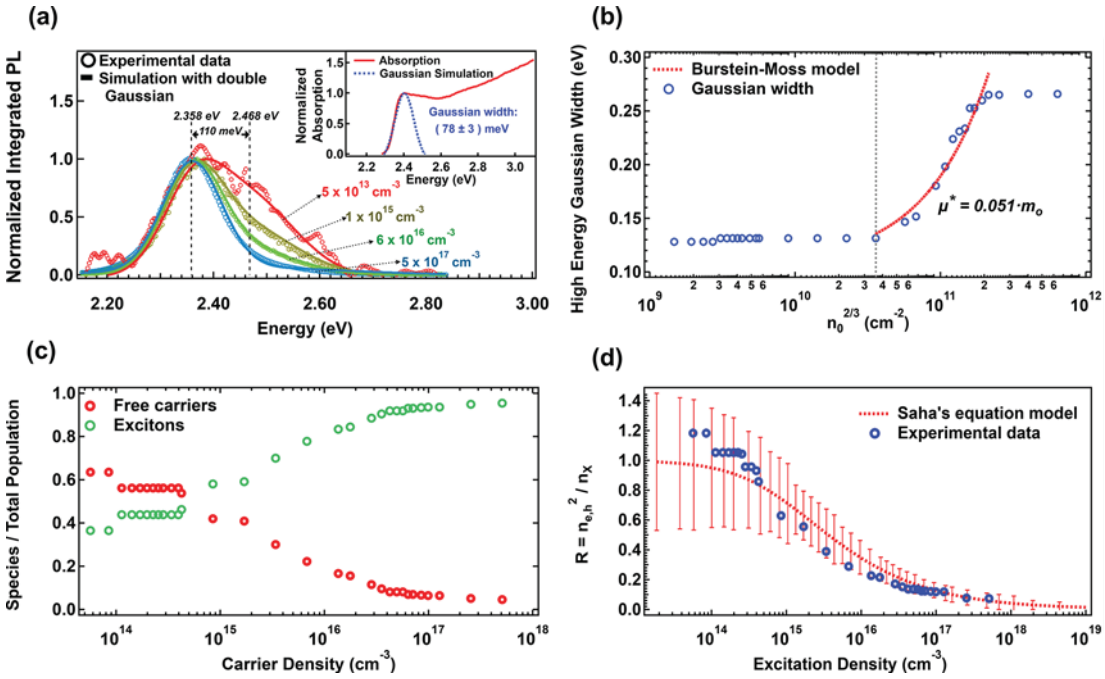

Figure 2. (a) Time-integrated PL spectra obtained under different excitation densities and simulated by a double Gaussian function for the polycrystalline perovskite film. Absorption of the same sample, with the excitonic peak analyzed by a single Gaussian function, is shown in the inset. (b) Width of the high-energy Gaussian (w_2) versus $n_o^{2/3}$, analyzed by a linear equation. (c) Population of free carriers and excitons over the total population of the excited state. (d) Ratio of the squared population of free carriers over that of the excitons at different carrier densities. A theoretical model, with our experimentally derived values implemented into the Saha equation, is shown on the same graph, together with error bars.

continuous white light (WL) illumination (Figure S4). The observed spectral changes in the polycrystalline perovskite include a shift, a spectral narrowing, and a reduction of the PL intensity on the high-energy side of the spectrum at high excitation intensities. Analysis of the integrated PL spectra with a single Gaussian function was not satisfactory. The sum of two Gaussian functions (eq 1) was needed to reproduce the experimental PL spectra, suggesting the coexistence of two emission bands due to excitons and free charges (Figures 2a and S5).

$$I_{PL} = A\cdot e^{-[(E-E_1)/w_1]^2} + B\cdot e^{-[(E-E_2)/w_2]^2} \quad (1)$$

In eq 1, A and B are the amplitudes, E_1 and E_2 the energies of the maximum PL intensity, and w_1 and w_2 the widths of the low- and high-energy Gaussian, respectively. E_1, E_2, and the width of the low-energy Gaussian (w_1) were kept constant, while A, B, and the width of the high-energy Gaussian (w_2) were left as free parameters. w_1 was fixed to the value obtained by analyzing the excitonic peak present in the absorption spectrum of the polycrystalline sample with a single Gaussian (78 meV), as shown in the inset of Figure 2a. The very good agreement between the experimental low-energy PL band and the fit, as well as the small Stoke's shift of 49 meV, confirm the excitonic origin of this emission band.

The width of the high-energy Gaussian w_2, which we assign to free carrier emission, was found to increase only after a certain carrier density. This behavior is characteristic of the Burstein–Moss shift due to band filling with free carriers upon photoexcitation at increasing carrier densities.[29−33] Figure 2b shows the evolution of w_2 at different $n_o^{2/3}$, where n_o is the excitation density (Burstein–Moss analysis, eq 2).

$$\Delta E_g^{BM} = \frac{\hbar^2}{2\mu^*}(3\pi^2 n_o)^{2/3} \quad (2)$$

In eq 2, ΔE_g^{BM} is the change in the optical band gap, μ^* is the exciton reduced effective mass, and $\hbar$ is the reduced Planck constant.[32] From the slope of the high excitation density part of Figure 2b, a value of $0.051\cdot m_o$ for the reduced effective mass was extracted (m_o being the electron mass). This value is smaller but on the same order of magnitude compared to those from previous reports.[34−40] According to Manser et al.[32] and Christians et al.,[33] the abrupt increase of w_2 that is observed at an excitation density of 7×10^{15} cm^{-3} ($n_o^{2/3} \approx 3.6 \times 10^{10}$ cm^{-2}) can be attributed to the process of trap filling (which competes with band filling at low excitation densities). This threshold can thus be used as a measure of the trap density in the material. The value is in agreement with the trap densities of polycrystalline perovskite films.[41] The plateau at higher excitation densities (>10^{17} cm^{-3}) is likely related to band gap renormalization, becoming more prominent due to the increased electron–electron interactions,[42,43] but also due to the decreased population of free carriers. Indeed, the emission spectra measured at high excitation densities become increasingly dominated by the excitonic band (Figure 2a).

By dividing the amplitudes of the two Gaussians by their sum, the relative population of the species contributing to each of the two emission bands at different excitation densities was estimated (Figure 2c). Already at the lowest excitation density, almost 40% of the excited species are excitons. At higher excitation densities, the exciton population increases while the free carrier population decreases almost to zero. This is an indication of the favored conversion of free carriers to excitons at high excitation densities, which results in inversion of the majority population in the excited state. This conversion has

been previously observed for $MAPbBr_3$,[14,15] and other perovskite materials.[44] As a consequence, the energy difference between the maximum PL intensity of the two Gaussians can be used to estimate the exciton binding energy to 110 meV, in agreement with previously reported values for $MAPbBr_3$ (ranging between 35 and 320 meV, depending on the crystal size and the dimensionality).[14,37,38,45,46] The value is further influenced by the chemical environment and dielectric constant of the surroundings.[47−49]

Figure 2d shows the ratio of the squared free-carrier population over the population of excitons. The Saha equation (eq 3), correlating this ratio of free carriers and excitons to the excitation density in hot electron−hole plasma, was used to model the obtained data.[5,29,44,50,51]

$$R = \frac{n_{e,h}^{\ 2}}{n_X} = \frac{1}{n}\left(\frac{2\pi\mu^* k_B T}{h^2}\right)^{3/2} e^{-E_B/k_B T} \tag{3}$$

In eq 3, $n_{e,h}$ is the population of free carriers and n_X is the population of excitons, both divided by their sum, which accounts for the total population. μ^* is the exciton reduced effective mass (estimated with the Burstein−Moss model), k_B is the Boltzmann constant, h is the Planck constant, T the temperature in Kelvin, and E_B the exciton binding energy of 110 meV. The calculation of the uncertainties of each parameter contributing to the error bars shown in Figure 2d is reported in the SI. The good agreement of the experimental data with the Saha model confirms the coexistence of free carriers and excitons in polycrystalline $MAPbBr_3$ thin films, even at low carrier densities. This is important as this carrier concentration range corresponds to the working regime of optoelectronic devices, such as LEDs and solar cells.[52]

In contrast to the polycrystalline perovskite, neither the microcrystals nor the nanocrystals show any variation in the shape of the integrated PL spectrum with increasing excitation density (Figure S2). This indicates that only a single excited species, which we assign to excitons, governs the emission. The direct formation of excitons upon photoexcitation is expected to be enhanced for the nanocrystals compared to the polycrystalline perovskite because of the weak quantum confinement. A larger exciton binding energy that favors the formation of excitons upon photoexcitation has also been observed for small $MAPbBr_3$ crystals even outside of the quantum confinement regime.[53] Changes in the dielectric environment due to the high volumetric fraction of the additive might enhance this effect (Table S1). This justifies an enhanced excitonic character for both the nano- and microcrystals. The higher electron−hole coupling for radiative excitonic recombination also explains the higher oscillator strength of the emission (higher k_{rad}, Table 1) compared to the polycrystalline perovskite, where both excitons and free charges contribute to the emission. In agreement, k_{rad} is highest in the nanocrystals (highest binding energy due to the weak confinement).

Further evidence that both excitons and free carriers are present in the polycrystalline perovskite while excitons are predominant for the micro- and nanocrystals is shown in Figure 3. This depicts the fluence dependence of the excited-state population rate, which can be described by a polynomial function containing the generation rate G_0 and decay rates of different orders (k_1, k_2, and k_3); see eq 4.

$$-\frac{dn}{dt} = -G_0 + k_1 n + k_2 n^2 + k_3 n^3 \tag{4}$$

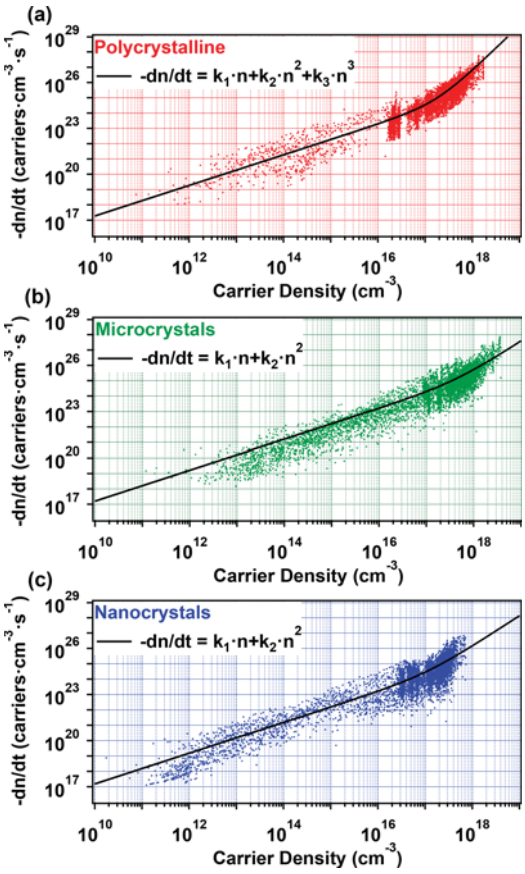

Figure 3. Population rate versus carrier density derived from ns-TRPL, ns-TA, and fs-TA measurements for the three systems. The black line represents an analysis with a third-order polynomial for the case of the polycrystalline perovskite (a) and with a second-order polynomial in the case of the microcrystals (b) and the nanocrystals (c).

Here, n is the density of either free carriers or of excitons, and it has been shown that the recombination terms in a free carrier semiconductor have different origins compared to excitonic materials.[54−56] For free carriers, k_1 is the monomolecular decay indicative of free carrier trapping, k_2 is the bimolecular electron−hole emission, and k_3 is the three-body Auger recombination term.[57−59] In the case of an excitonic semiconductor, k_1 represents the monomolecular excitonic and/or trap-assisted recombination and k_2 the exciton−exciton annihilation.[60−63] The third-order term k_3 is absent because there are no free carriers formed upon photoexcitation,[63] although it might become relevant if excitons dissociate to free carriers.

By combining data from nanosecond-resolved TRPL with nano- and femtosecond transient absorption (TA) spectroscopy (450 nm excitation), dn/dt was obtained over a broad regime of excitation densities and time scales, as shown in Figure 3 (see the SI and Figure S6 for details). The number of polynomial terms necessary to describe the data for the different samples provides information about the recombination process. We found above that both excitons and free carriers coexist in polycrystalline $MAPbBr_3$. In agreement, a complete description of the recombination rates can be obtained using three polynomial terms. For the micro- and nanocrystals containing only excitons, two polynomial terms are sufficient. The smaller $k_{n.rad}$ compared to k_{rad} (Table 1)

Table 2. Polynomial Coefficients Obtained by the Analysis of the Data Shown in Figure 3 by a Second- or Third-Order Polynomial Function

sample	polynomial order	$k_1 \times 10^7$ (s^{-1})	$k_2 \times 10^{-10}$ ($cm^3 \cdot s^{-1}$)	$k_3 \times 10^{-28}$ ($cm^6 \cdot s^{-1}$)
polycrystalline perovskite	3rd	1.8 ± 0.8	1.0 ± 0.9	5.3 ± 0.2
microcrystals	2nd	1.6 ± 0.2	0.37 ± 0.02	
nanocrystals	2nd	1.5 ± 0.2	1.3 ± 0.1	

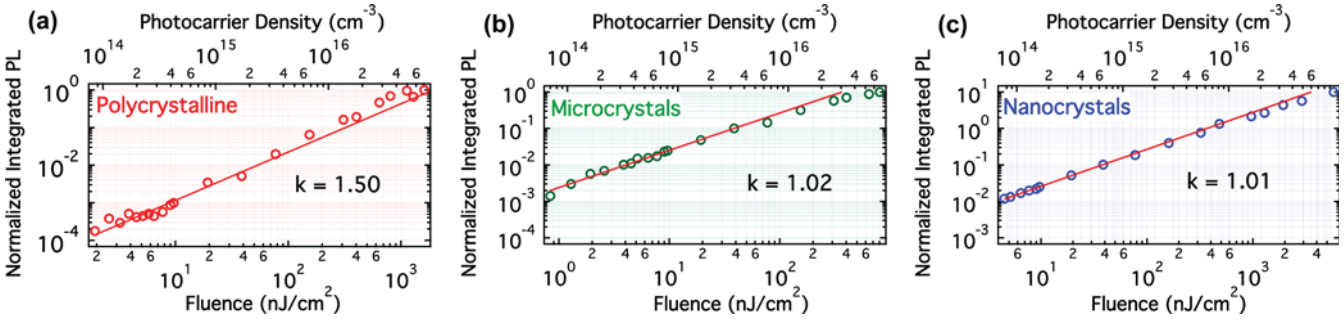

Figure 4. Graphs of the time-integrated PL intensity (at the spectral maximum) versus the excitation density (or fluence) for (a) the polycrystalline perovskite, (b) the microcrystals, and (c) the nanocrystals.

suggests that the radiative recombination of the excitons is more efficient compared to monomolecular trapping, thus governing the monomolecular term (see discussion below), while exciton−exciton annihilation governs the bimolecular term. The rate constants that were derived by the aforementioned analysis are reported in Table 2.

The values obtained for the polycrystalline films are in agreement with values reported for $MAPbBr_3$ by Yang et al.[64] but are higher than those observed by Richter et al.,[12] which we attribute to different preparation conditions. The higher monomolecular recombination rate that we observe in $MAPbBr_3$ compared to that for free carrier perovskites such as $MAPbI_3$[52,57] can be explained considering that not only monomolecular trapping but also excitonic recombination takes place in this material (we have shown the coexistence of the two species). The value of k_1 is almost the same for all investigated samples. Either excitonic recombination or trapping is included in this monomolecular term. We will show that excitonic recombination becomes more important with the reduction of the crystal size, while trapping becomes less pronounced, resulting in the increased contribution of radiative recombination for the micro- and nanocrystals (Table 1). The bimolecular recombination constant, k_2, is smaller for the microcrystals compared to that for the polycrystalline sample as it reflects only exciton−exciton annihilation and not free carrier recombination. The larger k_2 for the nanocrystals compared to the microcrystals is due to the enhanced exciton−exciton annihilation because of their spatial confinement. Despite the increase in k_2, it is still lower compared to that of other perovskite nanocrystals.[65] Importantly, the fact that the third-order polynomial term, including the three-body Auger recombination, is not necessary for the micro- and nanocrystals indicates that excitons created directly upon photoexcitation are stable and do not dissociate to free carriers even at high excitation fluencies. The generation of stable excitons was also shown by Sarritzu et al. in $MAPbBr_3$ crystals.[15]

To further investigate the recombination mechanism in the $MAPbBr_3$ thin films, the time-integrated PL intensity (at the spectral maximum) was plotted as a function of the excitation density (Figure 4; only data below the threshold of exciton−exciton annihilation and Auger recombination is shown). The result was analyzed with a power law function of the form $PL \approx F^k$, where F is the excitation fluence or density and k is a real number exponent, which provides information about the order of the recombination process.[13,66,67] In the polycrystalline perovskite, the value of 1.5 agrees with the coexistence of free carriers (bimolecular emission) and excitons (monomolecular emission) and with other measurements on perovskite thin films.[13] For the microcrystals and nanocrystals, the dependence of the integrated PL intensity on the excitation density becomes linear ($k \approx 1$), indicating predominantly monomolecular recombination. Similar behavior was observed when plotting PL_0, the maximum of the PL decay trace at t_0 within our 3 ns time resolution, as a function of fluence (Figure S3), confirming the above-mentioned results and the photostability of the samples (the PL_0 data was obtained with the same samples right after the time-integrated PL measurements). The monomolecular recombination in the micro- and nanocrystals could originate from either excitonic recombination (radiative) or trap-assisted recombination (nonradiative).[68] To distinguish between the two, the TRPL dynamics were recorded under different excitation densities.

For the polycrystalline sample (Figure 5a), the dynamics become slower as the excitation density increases until a value of 7×10^{15} cm^{-3}. According to analysis with the Burstein−Moss equation (Figure 2b), this excitation density coincides with the one for which traps are filled. By further increasing the excitation density, the dynamics become faster again (inset of Figure 5a) due to higher-order interactions such as Auger recombination. A similar trend has been observed in previous studies.[59,69,70] We note that nonreversible behavior of the TRPL dynamics when increasing and decreasing the excitation density has been reported due to photoinduced changes of the sample (e.g., photoinduced trap formation or ion migration).[71,72] We could exclude a significant contribution of such effects here because the emission properties were reproducible and did not change in the presence of continuous white light illumination (see Figures S3 and S4 and the discussion in the SI). To explain the slower dynamics upon trap filling, we consider a distribution of trap states as suggested by Yamada et al.[69] and Wright et al.[73] Filling of the trap states that lie deep in the bandgap (and that cause nonradiative recombination)

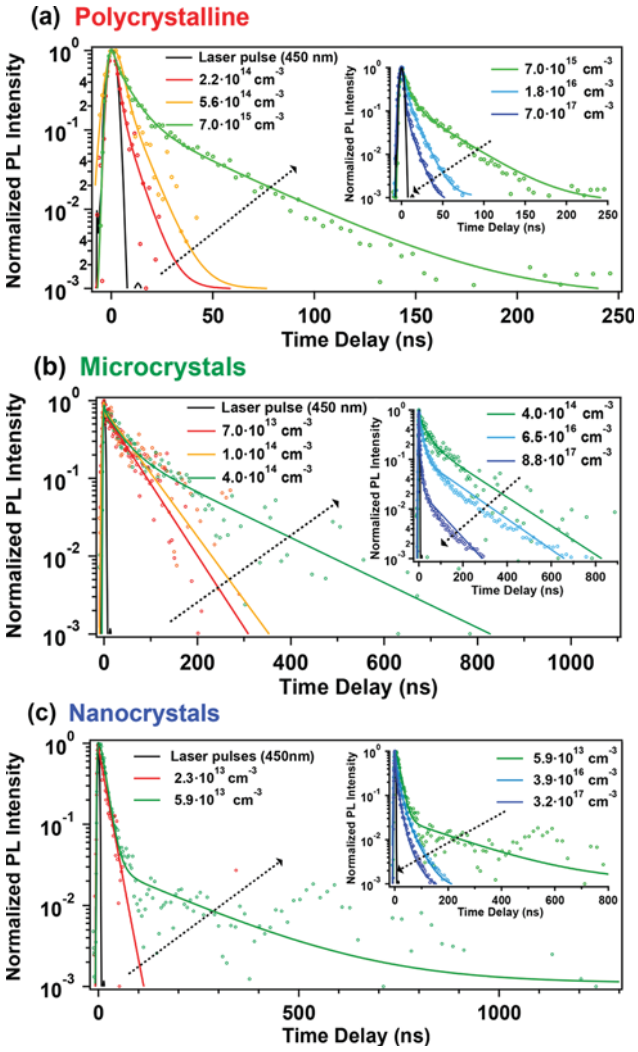

Figure 5. TRPL dynamics of (a) the polycrystalline perovskite, (b) the microcrystals, and (c) the nanocrystals obtained at different excitation densities with excitation at 450 nm with pulses of 3 ns duration and a repetition rate of 10 Hz. The insets show the PL dynamics recorded at high excitation densities where the dependence of the lifetime on the excitation density is opposite than the one observed at low excitation densities. The arrows indicate an increase in the excitation density.

leaves only shallow traps unfilled. Chirvony et al. showed that carriers temporarily trapped in the shallow states can be thermally detrapped, leading to delayed PL[74] and explaining the long-lived (hundreds of ns) tail in the PL dynamics at intermediate fluences. We have used the carrier density for which the inversion of the dynamics takes place to estimate a trap density of 4×10^{14} cm^{-3} for the microcrystals and of 5.9×10^{13} cm^{-3} for the nanocrystals (Figure 5b,c). These values are much smaller compared to polycrystalline $MAPbBr_3$, suggesting that these materials have little traps and are therefore suitable candidates for applications in LEDs.[68]

The reduction in trap density between the polycrystalline sample and the films with reduced crystal size is consistent with the strong reduction of $k_{n.rad}$ (Table 1). It shows that the monomolecular recombination in the latter samples is predominantly excitonic. It also explains the slower PL decay in the micro- and nanocrystals in Figure 2b. In the polycrystalline perovskite, the deep traps are filled at excitation densities where higher-order effects are already significantly present and reduce the overall excited-state lifetime. In contrast, delayed PL is seen more effectively at lower fluences in the systems with reduced crystal size. It is worth mentioning that the reduction of the crystal size of $MAPbBr_3$ should in fact lead to an increase of surface trap density due to the higher surface to volume ratio of smaller structures.[75] However, the additives present in the micro- and nanocrystals apparently passivate the surface traps, leading to reduced trap density. This then enhances the PLQY by reducing $k_{n.rad}$ and by favoring delayed PL. Finally, it is worth mentioning that the improved film morphology with the reduction of crystal size could also result in better out-coupling of the emitted light, as shown by Richter et al.[12] Although this factor cannot be excluded, it would not affect the nature of the emissive state and the PL lifetime, as we report here.

In summary, the origin of the PL in polycrystalline $MAPbBr_3$, as well as in micrometer- and nanometer-sized perovskite crystals, has been studied. By combining both time-integrated PL, time-resolved PL, and TA techniques, a broad range of excitation densities could be accessed. The results show that both free carriers and excitons coexist in the polycrystalline perovskite and that free carriers are converted into excitons at high excitation densities. On the other hand, in the micro- and nanocrystals, directly photogenerated excitons are predominant. The contributions of nonradiative trapping and radiative exciton recombination upon crystal size reduction was studied. We found that the excitonic character is enhanced with the size reduction, while trapping is suppressed. Thus, the large increase of the PLQY for micro- and nanocrystals is attributed to a combination of increased oscillator strength of the radiative transition due to the purely excitonic character of these materials and of reduction of the surface traps by passivation induced by the additives.

■ ASSOCIATED CONTENT

Supporting Information

The Supporting Information is available free of charge on the ACS Publications website at DOI: 10.1021/acsenergylett.8b00475.

Experimental details (sample preparation, steady-state absorption and PL techniques, ns-TRPL, and ns- and fs-TA experiments), SEM and TEM pictures, calculation of the excitation densities, table with the contents of the additive in each sample and its ratio with the perovskite, time-integrated PL measurements, integrated PL spectra of the polycrystalline perovskite analyzed with a double Gaussian function, calculation of errors accompanying the Saha model and tables with the uncertainties of each parameter, graphs of the PL_0 at different fluencies, graphs with the raw data from combined ns-TRPL/TA and fs-TA measurements, and TRPL measurements under different conditions of illumination (PDF)

■ AUTHOR INFORMATION

Corresponding Author

*E-mail: natalie.banerji@dcb.unibe.ch.

ORCID

Nikolaos Droseros: 0000-0002-9818-9387
Michele Sessolo: 0000-0002-9189-3005
Henk J. Bolink: 0000-0001-9784-6253
Natalie Banerji: 0000-0001-9181-2642

Present Address
[§]N.B.: Department of Chemistry and Biochemistry, University of Bern, Freiestrasse 3, CH-3012 Bern, Switzerland.

Notes
The authors declare no competing financial interest.

■ ACKNOWLEDGMENTS

This work has received funding from the European Research Council (ERC) under the European Union's Horizon 2020 research and innovation program INFORM (Grant Agreement N° 675867), the Spanish Ministry of Economy and Competitiveness (MINECO) via the Unidad de Excelencia María de Maeztu MDM-2015-0538 and MAT2014-55200, PCIN-2015-255, and the Generalitat Valenciana (Prometeo/2012/053). M.S. thanks the MINECO for his RyC contract. N.D., J.B., and N.B. would like to acknowledge the Universities of Fribourg and Bern, Switzerland, for providing funding and infrastructure.

■ REFERENCES

(1) Kojima, A.; Teshima, K.; Shirai, Y.; Miyasaka, T. Organometal Halide Perovskites as Visible-Light Sensitizers For Photovoltaic Cells. *J. Am. Chem. Soc.* **2009**, *131*, 6050−6051.
(2) Lee, M. M.; Teuscher, J.; Miyasaka, T.; Murakami, T. N.; Snaith, H. J. Efficient Hybrid Solar Cells Based On Meso-Superstructured Organometal Halide Perovskites. *Science* **2012**, *338*, 643−647.
(3) Kim, H.-S.; Lee, C.-R.; Im, J.-H.; Lee, K.-B.; Moehl, T.; Marchioro, A.; Moon, S.-J.; Humphry-Baker, R.; Yum, J.-H.; Moser, J. E.; et al. Lead Iodide Perovskite Sensitized All-Solid-State Submicron Thin Film Mesoscopic Solar Cell With Efficiency Exceeding 9%. *Sci. Rep.* **2012**, *2*, 591.
(4) Yantara, N.; Bhaumik, S.; Yan, F.; Sabba, D.; Dewi, H. A.; Mathews, N.; Boix, P. P.; Demir, H. V.; Mhaisalkar, S. Inorganic Halide Perovskites For Efficient Light-Emitting Diodes. *J. Phys. Chem. Lett.* **2015**, *6*, 4360−4364.
(5) Manser, J. S.; Christians, J. A.; Kamat, P. V. Intriguing Optoelectronic Properties Of Metal Halide Perovskites. *Chem. Rev.* **2016**, *116*, 12956−13008.
(6) Stranks, S. D.; Snaith, H. J. Metal-Halide Perovskites For Photovoltaic And Light-Emitting Devices. *Nat. Nanotechnol.* **2015**, *10*, 391−402.
(7) Kim, Y.-H.; Cho, H.; Lee, T.-W. Metal Halide Perovskite Light Emitters. *Proc. Natl. Acad. Sci. U. S. A.* **2016**, *113*, 11694−11702.
(8) Sutherland, B. R.; Sargent, E. H. Perovskite Photonic Sources. *Nat. Photonics* **2016**, *10*, 295−302.
(9) Longo, G.; La-Placa, M.-G.; Sessolo, M.; Bolink, H. J. High Photoluminescence Quantum Yields In Organic Semiconductor-Perovskite Composite Thin Films. *ChemSusChem* **2017**, *10*, 3788−3793.
(10) La-Placa, M.-G.; Longo, G.; Babaei, A.; Martínez-Sarti, L.; Sessolo, M.; Bolink, H. J. Photoluminescence Quantum Yield Exceeding 80% In Low Dimensional Perovskite Thin-Films Via Passivation Control. *Chem. Commun.* **2017**, *53*, 8707−8710.
(11) Xiao, Z.; Kerner, R. A.; Zhao, L.; Tran, N. L.; Lee, K. M.; Koh, T. W.; Scholes, G. D.; Rand, B. P. Efficient Perovskite Light-Emitting Diodes Featuring Nanometre-Sized Crystallites. *Nat. Photonics* **2017**, *11*, 108−115.
(12) Richter, J. M.; Abdi-Jalebi, M.; Sadhanala, A.; Tabachnyk, M.; Rivett, J. P. H.; Pazos-Outón, L. M.; Gödel, K. C.; Price, M.; Deschler, F.; Friend, R. H. Enhancing Photoluminescence Yields In Lead Halide Perovskites By Photon Recycling And Light Out-Coupling. *Nat. Commun.* **2016**, *7*, 13941.
(13) He, H.; Yu, Q.; Li, H.; Li, J.; Si, J.; Jin, Y.; Wang, N.; Wang, J.; He, J.; Wang, X.; et al. Exciton Localization In Solution-Processed Organolead Trihalide Perovskites. *Nat. Commun.* **2016**, *7*, 10896.
(14) Zheng, K.; Zhu, Q.; Abdellah, M.; Messing, M. E.; Zhang, W.; Generalov, A. V.; Niu, Y.; Ribaud, L.; Canton, S. E.; Pullerits, T. Exciton Binding Energy And The Nature Of Emissive States In Organometal Halide Perovskites. *J. Phys. Chem. Lett.* **2015**, *6*, 2969−2975.
(15) Sarritzu, V.; Sestu, N.; Marongiu, D.; Chang, X.; Wang, Q.; Loi, M. A.; Quochi, F.; Saba, M.; Mura, A.; Bongiovanni, G. Perovskite Excitonics: Primary Exciton Creation And Crossover From Free Carriers To A Secondary Exciton Phase. *Adv. Opt. Mater.* **2018**, *6*, 1700839.
(16) Stranks, S. D.; Burlakov, V. M.; Leijtens, T.; Ball, J. M.; Goriely, A.; Snaith, H. J. Recombination Kinetics In Organic-Inorganic Perovskites: Excitons, Free Charge, and Subgap States. *Phys. Rev. Appl.* **2014**, *2*, 034007.
(17) Draguta, S.; Thakur, S.; Morozov, Y. V.; Wang, Y.; Manser, J. S.; Kamat, P. V.; Kuno, M. Spatially Non-Uniform Trap State Densities In Solution-Processed Hybrid Perovskite Thin Films. *J. Phys. Chem. Lett.* **2016**, *7*, 715−721.
(18) Guo, Y.; Shoyama, K.; Sato, W.; Nakamura, E. Polymer Stabilization of Lead(II) Perovskite Cubic Nanocrystals for Semi-transparent Solar Cells. *Adv. Energy Mater.* **2016**, *6*, 1502317.
(19) Tanaka, K.; Takahashi, T.; Ban, T.; Kondo, T.; Uchida, K.; Miura, N. Comparative Study In The Excitons In Lead- Halide Based Perovskite-Type Crystals $CH_3NH_3PbBr_3$ $CH_3NH_3PbI_3$. *Solid State Commun.* **2003**, *127*, 619−623.
(20) Malgras, V.; Tominaka, S.; Ryan, J. W.; Henzie, J.; Takei, T.; Ohara, K.; Yamauchi, Y. Observation Of Quantum Confinement In Monodisperse Methylammonium Lead Halide Perovskite Nanocrystals Embedded In Mesoporous Silica. *J. Am. Chem. Soc.* **2016**, *138*, 13874−13881.
(21) Kayanuma, Y. Quantum-Size Effects Of Interacting Electrons And Holes In Semiconductor Microcrystals With Spherical Shape. *Phys. Rev. B: Condens. Matter Mater. Phys.* **1988**, *38*, 9797−9805.
(22) Scholes, G. D.; Rumbles, G. Excitons In Nanoscale Systems. *Nat. Mater.* **2006**, *5*, 920−920.
(23) Grancini, G.; Marras, S.; Prato, M.; Giannini, C.; Quarti, C.; De Angelis, F.; De Bastiani, M.; Eperon, G. E.; Snaith, H. J.; Manna, L.; et al. The Impact Of The Crystallization Processes On The Structural And Optical Properties Of Hybrid Perovskite Films For Photovoltaics. *J. Phys. Chem. Lett.* **2014**, *5*, 3836−3842.
(24) D'Innocenzo, V.; Srimath Kandada, A. R.; De Bastiani, M.; Gandini, M.; Petrozza, A. Tuning The Light Emission Properties By Band Gap Engineering In Hybrid Lead Halide Perovskite. *J. Am. Chem. Soc.* **2014**, *136*, 17730−17733.
(25) de Quilettes, D. W.; Vorpahl, S. M.; Stranks, S. D.; Nagaoka, H.; Eperon, G. E.; Ziffer, M. E.; Snaith, H. J.; Ginger, D. S. Impact Of Microstructure On Local Carrier Lifetime In Perovskite Solar Cells. *Science* **2015**, *348*, 683−686.
(26) Yuan, H.; Debroye, E.; Bladt, E.; Lu, G.; Keshavarz, M.; Janssen, K. P. F.; Roeffaers, M. B. J.; Bals, S.; Sargent, E. H.; Hofkens, J. Imaging Heterogeneously Distributed Photo-Active Traps in Perovskite Single Crystals. *Adv. Mater.* **2018**, *30*, 1705494.
(27) Diab, H.; Arnold, C.; Lédée, F.; Trippé-Allard, G.; Delport, G.; Vilar, C.; Bretenaker, F.; Barjon, J.; Lauret, J.-S.; Deleporte, E.; et al. Impact Of Reabsorption On The Emission Spectra And Recombination Dynamics Of Hybrid Perovskite Single Crystals. *J. Phys. Chem. Lett.* **2017**, *8*, 2977−2983.
(28) Wenger, B.; Nayak, P. K.; Wen, X.; Kesava, S. V.; Noel, N. K.; Snaith, H. J. Consolidation of the Optoelectronic Properties of $CH_3NH_3PbBr_3$ Perovskite Single Crystals. *Nat. Commun.* **2017**, *8*, 590.
(29) Wang, W.; Li, Y.; Wang, X.; Lv, Y.; Wang, S.; Wang, K.; Shi, Y.; Xiao, L.; Chen, Z.; Gong, Q. Density-Dependent Dynamical Coexistence of Excitons and Free Carriers In The Organolead Perovskite $CH_3NH_3PbI_3$. *Phys. Rev. B: Condens. Matter Mater. Phys.* **2016**, *94*, 1−5.
(30) Deschler, F.; Price, M.; Pathak, S.; Klintberg, L. E.; Jarausch, D. D.; Higler, R.; Hüttner, S.; Leijtens, T.; Stranks, S. D.; Snaith, H. J.; et al. High Photoluminescence Efficiency And Optically Pumped Lasing In Solution-Processed Mixed Halide Perovskite Semiconductors. *J. Phys. Chem. Lett.* **2014**, *5*, 1421−1426.

(31) Muñoz, M.; Pollak, F. H.; Kahn, M.; Ritter, D.; Kronik, L.; Cohen, G. M. Burstein-Moss Shift Of N-Doped In0.53Ga0.47As/InP. *Phys. Rev. B: Condens. Matter Mater. Phys.* **2001**, *63*, 233302.
(32) Manser, J. S.; Kamat, P. V. Band Filling With Free Charge Carriers In Organometal Halide Perovskites. *Nat. Photonics* **2014**, *8*, 737−743.
(33) Christians, J. A.; Manser, J. S.; Kamat, P. V. Multifaceted Excited State Of $CH_3NH_3PbI_3$. Charge Separation, Recombination, And Trapping. *J. Phys. Chem. Lett.* **2015**, *6*, 2086−2095.
(34) Yu, Z. G. Effective-Mass Model And Magneto-Optical Properties In Hybrid Perovskites. *Sci. Rep.* **2016**, *6*, 1−14.
(35) Miyata, A.; Mitioglu, A.; Plochocka, P.; Portugall, O.; Wang, J. T. W.; Stranks, S. D.; Snaith, H. J.; Nicholas, R. J. Direct Measurement Of The Exciton Binding Energy And Effective Masses For Charge Carriers In Organic-Inorganic Tri-Halide Perovskites. *Nat. Phys.* **2015**, *11*, 582−587.
(36) Ziffer, M. E.; Mohammed, J. C.; Ginger, D. S. Electroabsorption Spectroscopy Measurements Of The Exciton Binding Energy, Electron-Hole Reduced Effective Mass, And Band Gap In The Perovskite $CH_3NH_3PbI_3$. *ACS Photonics* **2016**, *3*, 1060−1068.
(37) Galkowski, K.; Mitioglu, A.; Miyata, A.; Plochocka, P.; Portugall, O.; Eperon, G. E.; Wang, J. T.-W.; Stergiopoulos, T.; Stranks, S. D.; Snaith, H. J.; et al. Determination Of The Exciton Binding Energy And Effective Masses For The Methylammonium And Formamidinium Lead Tri-Halide Perovskite Family. *Energy Environ. Sci.* **2016**, *9*, 962−970.
(38) Koutselas, I. B.; Ducasse, L.; Papavassiliou, G. C. Electronic Properties Of Three- And Low-Dimensional Semiconducting Materials With Pb Halide And Sn Halide Units. *J. Phys.: Condens. Matter* **1996**, *8*, 1217−1227.
(39) Giorgi, G.; Fujisawa, J. I.; Segawa, H.; Yamashita, K. Small Photocarrier Effective Masses Featuring Ambipolar Transport In Methylammonium Lead Iodide Perovskite: A Density Functional Analysis. *J. Phys. Chem. Lett.* **2013**, *4*, 4213−4216.
(40) Yu, M.; Yuan, S.; Wang, H.-Y.; Zhao, J.-S.; Qin, Y.; Fu, L.-M.; Zhang, J.-P.; Ai, X.-C. Characterization Of The Influences Of Morphology On The Intrinsic Properties Of Perovskite Films By Temperature-Dependent And Time-Resolved Spectroscopies. *Phys. Chem. Chem. Phys.* **2018**, *20*, 6575−6581.
(41) Stranks, S. D. Nonradiative Losses In Metal Halide Perovskites. *ACS Energy Lett.* **2017**, *2*, 1515−1525.
(42) Lebens-Higgins, Z.; Scanlon, D. O.; Paik, H.; Sallis, S.; Nie, Y.; Uchida, M.; Quackenbush, N. F.; Wahila, M. J.; Sterbinsky, G. E.; Arena, D. A.; et al. Direct Observation Of Electrostatically Driven Band Gap Renormalization In A Degenerate Perovskite Transparent Conducting Oxide. *Phys. Rev. Lett.* **2016**, *116*, 1−5.
(43) Saran, R.; Heuer-Jungemann, A.; Kanaras, A. G.; Curry, R. J. Giant Bandgap Renormalization And Exciton−Phonon Scattering In Perovskite Nanocrystals. *Adv. Opt. Mater.* **2017**, *5*, 1700231.
(44) D'Innocenzo, V.; Grancini, G.; Alcocer, M. J. P.; Kandada, A. R. S.; Stranks, S. D.; Lee, M. M.; Lanzani, G.; Snaith, H. J.; Petrozza, A. Excitons Versus Free Charges In Organo-Lead Tri-Halide Perovskites. *Nat. Commun.* **2014**, *5*, 3586.
(45) Sestu, N.; Cadelano, M.; Sarritzu, V.; Chen, F.; Marongiu, D.; Piras, R.; Mainas, M.; Quochi, F.; Saba, M.; Mura, A.; et al. Absorption F-Sum Rule For The Exciton Binding Energy In Methylammonium Lead Halide Perovskites. *J. Phys. Chem. Lett.* **2015**, *6*, 4566−4572.
(46) Soufiani, A. M.; Huang, F.; Reece, P.; Sheng, R.; Ho-baillie, A.; Green, M. A. Polaronic Exciton Binding Energy In Iodide And Bromide Organic-Inorganic Lead Halide Perovskites Polaronic Exciton Binding Energy In Iodide And Bromide Organic-Inorganic Lead Halide Perovskites. *Appl. Phys. Lett.* **2015**, *107*, 231902.
(47) Grancini, G.; Srimath Kandada, A. R.; Frost, J. M.; Barker, A. J.; De Bastiani, M.; Gandini, M.; Marras, S.; Lanzani, G.; Walsh, A.; Petrozza, A. Role Of Microstructure In The Electron-Hole Interaction Of Hybrid Lead Halide Perovskites. *Nat. Photonics* **2015**, *9*, 695−701.
(48) Zhang, W.; Saliba, M.; Stranks, S. D.; Sun, Y.; Shi, X.; Wiesner, U.; Snaith, H. J. Enhancement Of Perovskite-Based Solar Cells Employing Core − Shell Metal Nanoparticles. *Nano Lett.* **2013**, *13*, 4505−4510.
(49) Hsiao, Y.-C.; Wu, T.; Li, M.; Liu, Q.; Qin, W.; Hu, B. Fundamental Physics Behind High-Efficiency Organo-Metal Halide Perovskite Solar Cells. *J. Mater. Chem. A* **2015**, *3*, 15372−15385.
(50) Rossi, F. Coherent Phenomena In Semiconductors. *Semicond. Sci. Technol.* **1998**, *13*, 147−168.
(51) Cingolani, R.; Calcagnile, L.; Coli, G.; Rinaldi, R.; Lomoscolo, M.; DiDio, M.; Franciosi, a.; Vanzetti, L.; LaRocca, G. C.; Campi, D. Radiative Recombination Processes In Wide-Band-Gap II−VI Quantum Wells: The Interplay Between Excitons And Free Carriers. *J. Opt. Soc. Am. B* **1996**, *13*, 1268.
(52) Johnston, M. B.; Herz, L. M. Hybrid Perovskites For Photovoltaics: Charge-Carrier Recombination, Diffusion, And Radiative Efficiencies. *Acc. Chem. Res.* **2016**, *49*, 146−154.
(53) Zheng, K.; Zhu, Q.; Abdellah, M.; Messing, M. E.; Zhang, W.; Generalov, A.; Niu, Y.; Ribaud, L.; Canton, S. E.; Pullerits, T. Exciton Binding Energy And The Nature Of Emissive States In Organometal Halide Perovskites. *J. Phys. Chem. Lett.* **2015**, *6*, 2969−2975.
(54) Boiko, G. A.; Dneprovskii, S.; Kraevskii, M. V.; Marinova, K.; Oak, S. M.; Silina, E. K.; et al. A Study Of The Kinetics Of Recombination Radiation Of CdS And CdSe Crystals. *Phys. Status Solidi B* **1978**, *85*, 111−119.
(55) Haug, H.; Mengel, P. On The Relaxation Paths Of Electron-Hole Pairs In Highly Excited II-VI Semiconductors. *J. Lumin.* **1976**, *12-13*, 629−634.
(56) a la Guillaume, C. B.; Debever, J.; Salvan, F. Radiative Recombination In Highly Excited CdS. *Phys. Rev.* **1969**, *177*, 567−580.
(57) Wehrenfennig, C.; Eperon, G. E.; Johnston, M. B.; Snaith, H. J.; Herz, L. M. High Charge Carrier Mobilities And Lifetimes In Organolead Trihalide Perovskites. *Adv. Mater.* **2014**, *26*, 1584−1589.
(58) Milot, R. L.; Eperon, G. E.; Green, T.; Snaith, H. J.; Johnston, M. B.; Herz, L. M. Radiative Monomolecular Recombination Boosts Amplified Spontaneous Emission In $HC(NH_2)_2SnI_3$ Perovskite Films. *J. Phys. Chem. Lett.* **2016**, *7*, 4178−4184.
(59) Phuong, L. Q.; Braly, I. L.; Katahara, J. K.; Hillhouse, H. W.; Kanemitsu, Y. Nonlinear Photocarrier Recombination Dynamics In Mixed-Halide $CH_3NH_3Pb(I_{1-x}Br_x)_3$ Perovskite Thin Films. *Appl. Phys. Express* **2017**, *10*, 102401.
(60) Makarov, N. S.; Guo, S.; Isaienko, O.; Liu, W.; Robel, I.; Klimov, V. I. Spectral And Dynamical Properties Of Single Excitons, Biexcitons, And Trions In Cesium-Lead-Halide Perovskite Quantum Dots. *Nano Lett.* **2016**, *16*, 2349−2362.
(61) Yuan, L.; Huang, L. Exciton Dynamics And Annihilation In WS_2 2D Semiconductors. *Nanoscale* **2015**, *7*, 7402−7408.
(62) Surrente, A.; Mitioglu, A. A.; Galkowski, K.; Klopotowski, L.; Tabis, W.; Vignolle, B.; Maude, D. K.; Plochocka, P. Onset Of Exciton-Exciton Annihilation In Single-Layer Black Phosphorus. *Phys. Rev. B: Condens. Matter Mater. Phys.* **2016**, *94*, 3−8.
(63) Soavi, G.; Dal Conte, S.; Manzoni, C.; Viola, D.; Narita, A.; Hu, Y.; Feng, X.; Hohenester, U.; Molinari, E.; Prezzi, D.; et al. Exciton−exciton Annihilation And Biexciton Stimulated Emission In Graphene Nanoribbons. *Nat. Commun.* **2016**, *7*, 11010.
(64) Yang, Y.; Yang, M.; Li, Z.; Crisp, R.; Zhu, K.; Beard, M. C. Comparison Of Recombination Dynamics In CH3NH3PbBr3 And CH3NH3PbI3 Perovskite Films: Influence Of Exciton Binding Energy. *J. Phys. Chem. Lett.* **2015**, *6*, 4688−4692.
(65) Wei, K.; Zheng, X.; Cheng, X.; Shen, C.; Jiang, T. Observation Of Ultrafast Exciton−Exciton Annihilation In $CsPbBr_3$ Quantum Dots. *Adv. Opt. Mater.* **2016**, *4*, 1993−1997.
(66) Schmidt, T.; Lischka, K.; Zulehner, W. Excitation-Power Dependence Of The Near-Band-Edge Photoluminescence Of Semiconductors. *Phys. Rev. B: Condens. Matter Mater. Phys.* **1992**, *45*, 8989−8994.
(67) Shibata, H.; Sakai, M.; Yamada, A.; Matsubara, K.; Sakurai, K.; Tampo, H.; Ishizuka, S.; Kim, K. K.; Niki, S. Excitation-Power Dependence Of Free Exciton Photoluminescence Of Semiconductors. *Japanese J. Appl. Physics, Part 1 Regul. Pap. Short Notes Rev. Pap.* **2005**, *44*, 6113−6114.

(68) Xing, G.; Wu, B.; Wu, X.; Li, M.; Du, B.; Wei, Q.; Guo, J.; Yeow, E. K. L.; Sum, T. C.; Huang, W. Transcending The Slow Bimolecular Recombination In Lead-Halide Perovskites For Electroluminescence. *Nat. Commun.* **2017**, *8*, 14558.
(69) Yamada, Y.; Yamada, T.; Shimazaki, A.; Wakamiya, A.; Kanemitsu, Y. Interfacial Charge-Carrier Trapping In $CH_3NH_3PbI_3$-Based Heterolayered Structures Revealed By Time-Resolved Photoluminescence Spectroscopy. *J. Phys. Chem. Lett.* **2016**, *7*, 1972−1977.
(70) Handa, T.; Tex, D. M.; Shimazaki, A.; Wakamiya, A.; Kanemitsu, Y. Charge Injection Mechanism At Heterointerfaces In $CH_3NH_3PbI_3$ Perovskite Solar Cells Revealed By Simultaneous Time-Resolved Photoluminescence And Photocurrent Measurements. *J. Phys. Chem. Lett.* **2017**, *8*, 954−960.
(71) Motti, S. G.; Gandini, M.; Barker, A. J.; Ball, J. M.; Srimath Kandada, A. R.; Petrozza, A. Photoinduced Emissive Trap States In Lead Halide Perovskite Semiconductors. *ACS Energy Lett.* **2016**, *1*, 726−730.
(72) Chen, S.; Wen, X.; Huang, S.; Huang, F.; Cheng, Y.-B.; Green, M.; Ho-Baillie, A. Light Illumination Induced Photoluminescence Enhancement And Quenching In Lead Halide Perovskite. *Sol. RRL* **2017**, *1*, 1600001.
(73) Wright, A. D.; Milot, R. L.; Eperon, G. E.; Snaith, H. J.; Johnston, M. B.; Herz, L. M. Band-Tail Recombination In Hybrid Lead Iodide Perovskite. *Adv. Funct. Mater.* **2017**, *27*, 1700860.
(74) Chirvony, V. S.; González-Carrero, S.; Suárez, I.; Galian, R. E.; Sessolo, M.; Bolink, H. J.; Martínez-Pastor, J. P.; Pérez-Prieto, J. Delayed Luminescence In Lead Halide Perovskite Nanocrystals. *J. Phys. Chem. C* **2017**, *121*, 13381−13390.
(75) Demchyshyn, S.; Roemer, J. M.; Groiß, H.; Heilbrunner, H.; Ulbricht, C.; Apaydin, D.; Böhm, A.; Rütt, U.; Bertram, F.; Hesser, G.; et al. Confining Metal-Halide Perovskites In Nanoporous Thin Films. *Sci. Adv.* **2017**, *3*, e1700738.